

# Nanocomposite ceramics based on La-doped BaTi<sub>2</sub>O<sub>5</sub> and BaTiO<sub>3</sub> with high temperature-independent permittivity and low dielectric loss

Héctor Beltrán · Nahum Masó  
Eloisa Cordoncillo · Anthony R. West

Received: 11 January 2007 / Accepted: 4 April 2007 / Published online: 24 April 2007  
© Springer Science + Business Media, LLC 2007

**Abstract** Nanocomposite ceramics containing a mixture of two ferroelectric phases, La-doped BaTi<sub>2</sub>O<sub>5</sub> and BaTiO<sub>3</sub>, with carefully-controlled phase amounts and ceramic microstructure have temperature-independent permittivity and low dielectric loss over very wide temperature ranges:  $\epsilon' = 95 \pm 10$  from 25 to 600 °C;  $\tan \delta = 0.02(2)$  from 25 to 400 °C, measured at 100 kHz. Further optimisation of properties should be possible.

**Keywords** BaTi<sub>2</sub>O<sub>5</sub> · Ferroelectric · Nanocomposite · Permittivity · Sol-gel

## 1 Introduction

A new high temperature ferroelectric barium titanate, BaTi<sub>2</sub>O<sub>5</sub>, was discovered recently in Japan [1–4]. The permittivity of single crystals is very anisotropic with values of  $\sim 20,000$  in the direction of the polar *b* axis of the monoclinic cell, but much smaller values of  $\sim 100$  in directions perpendicular to the polar axis; the Curie temperature,  $T_c$ , is  $\sim 430$  °C. The electrical properties of sol-gel-derived ceramics show a permittivity maximum in the range  $\sim 120$ – $140$  at  $T_c$  [5].

BaTi<sub>2</sub>O<sub>5</sub> (BT<sub>2</sub>) is believed to be an entirely metastable phase. It does not appear on the latest version of the BaO–TiO<sub>2</sub> phase diagram [6], which avoids the question of the low temperature stability/metastability of BaTi<sub>2</sub>O<sub>5</sub> by not showing phase relations below 1,200 °C. BaTi<sub>2</sub>O<sub>5</sub> can be obtained by several methods: by quenching eutectic melts from above 1,320 °C [7]; as single crystals grown from melts [1–4, 8, 9]; by low temperature sol-gel synthesis [10–13]. It cannot be prepared by standard solid state reaction routes with heating at e.g., 1,100–1,300 °C. On heating sol-gel-derived samples at higher temperatures,  $\geq 1,150$  °C, BT<sub>2</sub> decomposes to give a mixture of BaTiO<sub>3</sub> (BT) and Ba<sub>6</sub>Ti<sub>17</sub>O<sub>40</sub> (B<sub>6</sub>T<sub>17</sub>). There was some evidence that the value of  $T_c$  in sol-gel derived ceramics varied somewhat over the range 450–470 °C, depending on sample heat treatment in air [5]; in addition, single crystals grown in reducing atmosphere had lower  $T_c$ ,  $\sim 400$  °C, than those grown in air,  $\sim 460$  °C [14, 15]. Possibly, therefore, BT<sub>2</sub> is capable of a significant, but limited variation in its stoichiometry, either Ba:Ti ratio and/or oxygen content.

With the discovery of this new ferroelectric phase, it is clearly of interest to carry out doping studies with a view to, for instance, modifying  $T_c$  and increasing its thermodynamic stability so as to make sample fabrication easier. It would also be of great interest to find dopants that can reduce the high anisotropy in the permittivity so that the permittivity of polycrystalline samples can be increased; however, this may not be possible since, unlike BT, the crystal structure of BT<sub>2</sub> is highly anisotropic above  $T_c$  as well as below  $T_c$ . An attractive feature of BT<sub>2</sub> for high temperature application possibilities is that, not only does it have high permittivity at high temperatures, but also, it has a low dielectric loss,  $\tan \delta$ , for temperatures up to 400 °C, whereas  $\tan \delta$  of BT increases significantly above  $\sim 200$  °C [16].

H. Beltrán (✉) · N. Masó · E. Cordoncillo  
Departamento de Química Inorgánica y Orgánica,  
Universidad Jaime I,  
Avda. Sos Baynat s/n,  
12071 Castellón, Spain  
e-mail: mir@qio.uji.es

A. R. West  
Department of Engineering Materials,  
The University of Sheffield,  
Mappin Street, Sheffield S1 3JD, UK

We report here an investigation into La-doped  $\text{BT}_2$  and the serendipitous discovery that, although relatively little La, <1%, is able to enter the  $\text{BT}_2$  crystal lattice, we have identified a new method to achieve high temperature-independent permittivity, coupled with low dielectric loss, over a very wide range of temperatures. This is achieved by the fabrication of nano-composite materials containing a mixture of  $\text{BT}_2$  and La-doped BT. Additional features of these new materials are that they are Pb-free and the sol–gel based synthesis method could be used for sample preparation in the form of films.

## 2 Experimental

Lanthanum-doped  $\text{BaTi}_2\text{O}_5$  samples were prepared by sol–gel synthesis.  $\text{Ba}(\text{CH}_3\text{COO})_2$  (99%),  $\text{La}(\text{CH}_3\text{COO})_3 \cdot 3/2\text{H}_2\text{O}$  (99.9%) and  $\text{Ti}(\text{C}_3\text{H}_7\text{O})_4$  (98%, with 2% iso-propanol), all Strem Chemicals, were used as starting reagents. The synthesis method was similar to the experimental procedure described earlier [17]. Air-dried gels were decomposed by heating at  $5\text{ }^\circ\text{C min}^{-1}$  to  $500\text{ }^\circ\text{C}$ , left at  $500\text{ }^\circ\text{C}$  for 1 h and then heated to  $1,100\text{ }^\circ\text{C}$  at a rate of  $5\text{ }^\circ\text{C min}^{-1}$  with a final hold at  $1,100\text{ }^\circ\text{C}$  for 2 h. Samples were cooled, crushed, pelleted, reheated at  $1,100\text{ }^\circ\text{C}$  for 2 h and then cooled slowly inside the furnace. At the outset, it was not known whether La could enter the crystal lattice of  $\text{BT}_2$  but if so,  $\text{La}^{3+}$  would substitute for similar-sized  $\text{Ba}^{2+}$ , with one of three plausible mechanisms of charge compensation to balance the charge difference between  $\text{La}^{3+}$  and  $\text{Ba}^{2+}$ . Three sets of compositions were therefore prepared with these three possible substitution mechanisms:

1. Titanium vacancy compensation on substitution of Ba by La and general formula  $\text{Ba}_{1-x}\text{La}_x\text{Ti}_{2-x/4}\text{O}_5$ .
2. Barium vacancy compensation with general formula  $\text{Ba}_{1-3x/2}\text{La}_x\text{Ti}_2\text{O}_5$ .
3. Direct donor doping with compensation either by creation of  $\text{Ti}^{3+}$  ions or interstitial oxygens and general formula  $\text{Ba}_{1-x}\text{La}_x\text{Ti}_2\text{O}_{5+\delta}$ .

For each series, three compositions were chosen with  $x=0.01$ ,  $0.02$  and  $0.03$ , as summarised in Table 1. Average pellet densities were estimated from pellet dimensions, mass and theoretical density, making the assumption that the samples were single-phase La-doped  $\text{BT}_2$ , according to the mechanisms given in Table 1. In fact, all samples were multiphase and accurate theoretical densities would require detailed knowledge of the relative amounts of the different phases present. Such calculations have not been carried out but, to a first approximation based on the assumptions made, average pellet density was estimated at  $\sim 74\%$  and was essentially independent of composition. Phases were identified by powder X-ray diffraction

**Table 1** Compositions studied and phases present by X-ray powder diffraction.

General composition	$x$	Label	Phases present by XRD <sup>a</sup>
$\text{Ba}_{1-x}\text{La}_x\text{Ti}_{2-x/4}\text{O}_5$	0.01	1.1	$\text{BT}_2/\text{BT}/\text{B}_6\text{T}_{17}$
	0.02	1.2	$\text{BT}_2/\text{BT}/\text{B}_6\text{T}_{17}$
	0.03	1.3	$\text{BT}/\text{B}_6\text{T}_{17}$
$\text{Ba}_{1-3x/2}\text{La}_x\text{Ti}_2\text{O}_5$	0.01	2.1	$\text{BT}_2/\text{BT}/\text{B}_6\text{T}_{17}$
	0.02	2.2	$\text{BT}_2/\text{BT}/\text{B}_6\text{T}_{17}$
	0.03	2.3	$\text{BT}/\text{B}_6\text{T}_{17}$
$\text{Ba}_{1-x}\text{La}_x\text{Ti}_2\text{O}_{5+\delta}$	0.01	3.1	$\text{BT}_2/\text{BT}/\text{B}_6\text{T}_{17}$
	0.02	3.2	$\text{BT}_2/\text{BT}/\text{B}_6\text{T}_{17}$
	0.03	3.3	$\text{BT}/\text{B}_6\text{T}_{17}$

<sup>a</sup> $\text{BT}_2=\text{BaTi}_2\text{O}_5$  [JCPDS n° 34-133];  $\text{BT}=\text{BaTiO}_3$  [JCPDS n° 5-626];  $\text{B}_6\text{T}_{17}=\text{Ba}_6\text{Ti}_{17}\text{O}_{40}$  [JCPDS n° 35-817]

(XRD) analysis using a Siemens D5000 diffractometer with  $\text{CuK}\alpha$  radiation.

Sample textures were analysed by Scanning Electron Microscopy (SEM) using a Leica SEM instrument, model Leo 440, equipped with a spectrometer for energy dispersion of X-ray analysis (EDX), using the following operation parameters: acceleration voltage 20 kV, measuring time 100 s, working distance 25 mm, counting rate 1.2 kcps. The samples for microstructural and microanalysis determination were deposited on an Al holder and coated with graphite.

For electrical property measurements, electrodes were fabricated on opposite pellet faces from Pt paste, which was dried and decomposed by gradually heating to  $900\text{ }^\circ\text{C}$ . Samples with electrodes attached were placed into a conductivity jig and electrical property data recorded using an Agilent 4294A impedance analyser over the frequency range, 40 Hz to 13 MHz and over the temperature range, room temperature to  $900\text{ }^\circ\text{C}$ . Impedance data were corrected for overall pellet geometry and for the blank cell capacitance ('jig correction'). An LCR impedance meter, Quadtech 1920, was used to make fixed frequency measurements of capacitance over the range room temperature to  $600\text{ }^\circ\text{C}$  with data recorded at several frequencies in the range  $10^3$  to  $10^5$  Hz.

## 3 Results and discussion

X-ray powder diffraction results for the nine samples fired at  $1,100\text{ }^\circ\text{C}$  for 2 h are summarised in Table 1. For all three series with  $x=0.01$ ,  $\text{BT}_2$  was the major phase and the amount of  $\text{BT}_2$  decreased for  $x=0.02$ ; for all compositions with  $x=0.03$ , phase mixtures of BT and  $\text{B}_6\text{T}_{17}$  were obtained with no indications of any  $\text{BT}_2$ . From the XRD results, there was no evidence for the presence of any separate La-containing phase, but the results of the

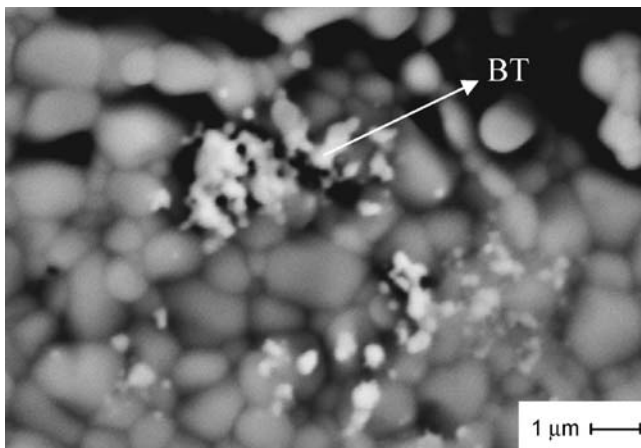


**Fig. 1** SEM micrograph of sample 1.1 sintered at 1,100 °C for 2 h

electrical property measurements, later, indicated that BT contained some La in solid solution formation.

An SEM photograph for sample 1.1 is shown in Fig. 1. This, together with SEM data for composition 1.2 (not shown) showed the presence of micron-sized grains of BT<sub>2</sub>, interspersed with particles of BT of approximate size 200 nm. At this stage, we do not know whether the fine

particles of BT were produced by direct crystallisation of the gel or formed by subsequent decomposition of BT<sub>2</sub> that had crystallised first at lower temperatures.

In order to assess the electrical microstructure of samples, variable frequency impedance data were obtained and are shown for one typical data set in the form of an impedance complex plane plot, Fig. 2(a), and spectroscopic plots of  $Z''$  and  $M''$  against log frequency, Fig. 2(b). The complex plane plot shows an undistorted, almost perfect semicircular arc, whereas the spectroscopic plots show single, almost Debye-like overlapping peaks. Interpretation of these data is that the sample can be represented by a single parallel RC element and therefore, the samples are essentially, electrically homogeneous. All samples showed a similar electrical response to that seen in Fig. 2.

Since the impedance data show that the electrical response can be represented by a single parallel RC element, the capacitance and hence permittivity values, are essentially independent of frequency. Permittivity data are therefore shown as a function of temperature at a fixed frequency of 100 kHz in Figs. 3 and 4 for composition series 1 and 2,

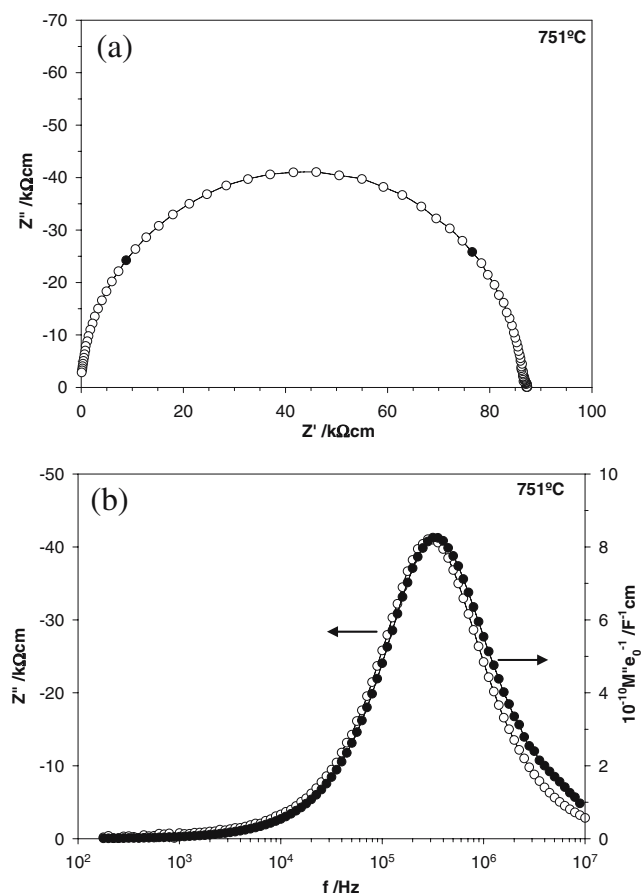


**Fig. 2** (a) Impedance complex plane,  $Z^*$ , and (b) impedance,  $Z''$ , and modulus,  $M''$ , spectroscopic plots at 751 °C for sample 1.2. The *solid data points* in (a) refer to frequencies of 100 kHz and 1 MHz

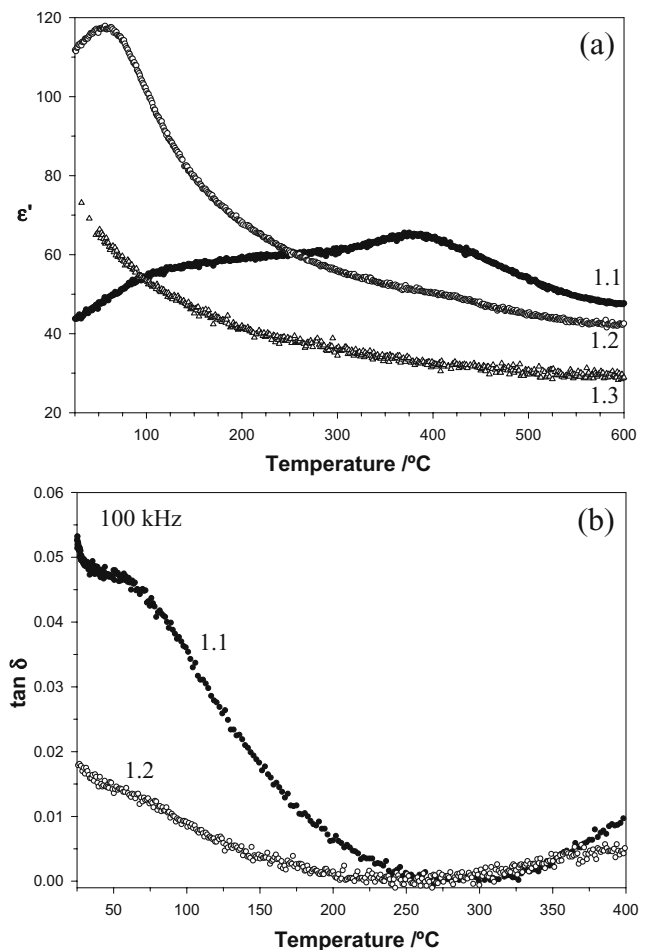


**Fig. 3** (a) Permittivity and (b)  $\tan \delta$  data as a function of temperature at 100 kHz for samples 1.1, 1.2 and 1.3

respectively, with a selection of corresponding  $\tan \delta$  data for the same samples.

Sample 1.1 shows a broad permittivity maximum at approximately 380 °C, somewhat lower than that of undoped  $\text{BT}_2$  430–470 °C [5], attributed to La-doped  $\text{BT}_2$ ; in sample 1.2, this maximum is smeared out and a second broad maximum in the range 50–70 °C is attributed to La-doped BT [18]. In sample 1.3, which no longer contained any  $\text{BT}_2$ , permittivity data show a rising value with decreasing temperature which has still not reached a maximum at room temperature and is attributed to La-doped BT with a higher La content.  $\tan \delta$  data show  $\tan \delta$  values=0.02(2) over a wide temperature range.

Sample 2.1 again shows a broad maximum at ~400 °C associated with La-doped  $\text{BT}_2$ , but this disappears from samples 2.2 and 2.3 for which the permittivity data are dominated by the low temperature, La-doped BT component, Fig. 4. Similar results were obtained for series 3 compositions (not shown).

From the impedance complex plane plots, the total sample resistance was obtained for each sample and is shown plotted in Arrhenius format for one series of

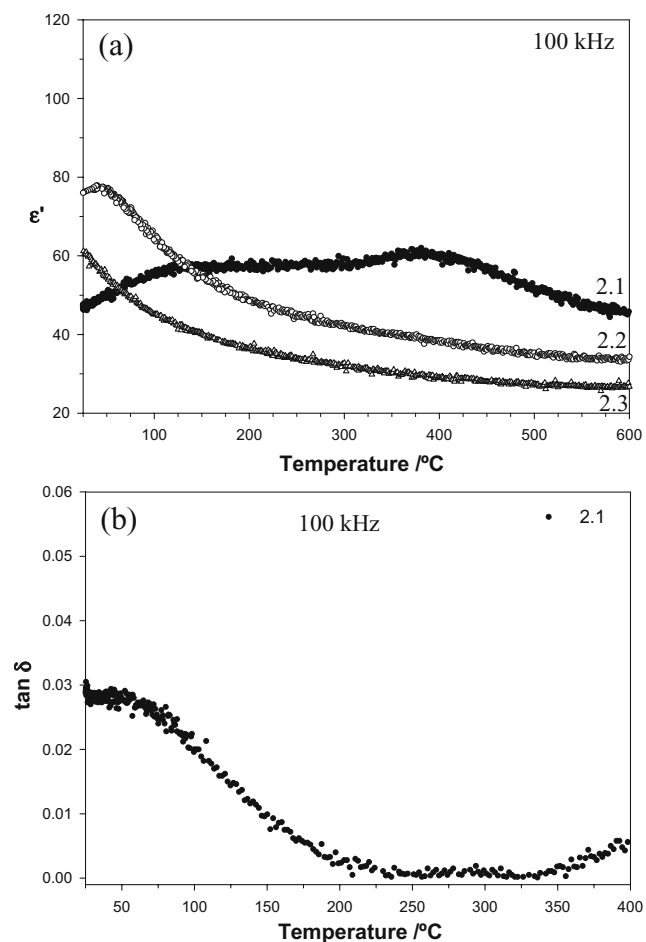


Fig. 4 (a) Permittivity and (b)  $\tan \delta$  data as a function of temperature at 100 kHz for samples 2.1, 2.2 and 2.3

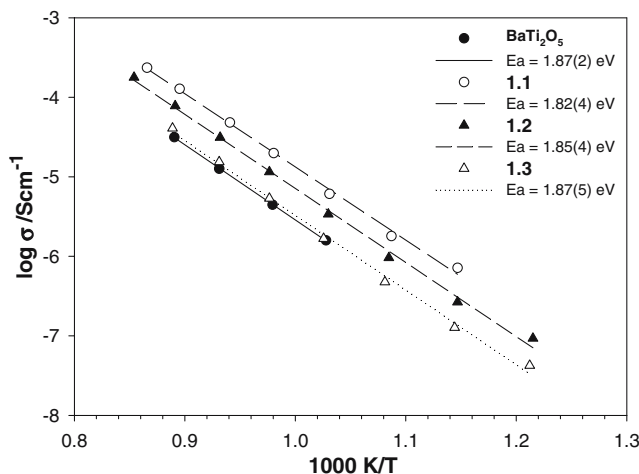


Fig. 5 Arrhenius plots of total conductivity for samples 1.1, 1.2 and 1.3; for comparison, data are shown for  $\text{BaTi}_2\text{O}_5$  [5]

compositions in Fig. 5. Linear plots were obtained with high activation energies, ~1.8 eV; all samples are highly insulating, even at high temperatures and show a very modest decrease in conductivity with increasing  $x$ . Similar behaviour was observed for series 2 and 3 (not shown).

In order to interpret the results in terms of phases, phase compositions and phase amounts in mixtures, the composition triangle,  $\text{BaO}-\text{TiO}_2-\text{La}_2\text{O}_3$  is shown in Fig. 6(a), on which are superposed the loci of the three composition series based on  $\text{BT}_2$ , with the three possible mechanisms (1) to (3) for substitution of La for Ba. Also shown is the locus of the La-doped BT solid solutions, (4), which form with a titanium vacancy compensation mechanism [18];  $T_c$  data obtained from reference 18 ( $T_c$  decreases at a rate of ~24 °C per at.% La) were used to obtain an estimate of the composition of the BT phase from the temperatures of the maxima in permittivity plots such as Figs. 3 and 4.

Since none of the nine samples studied contained phase-pure  $\text{BT}_2$ , it appears that the solubility limit of La in

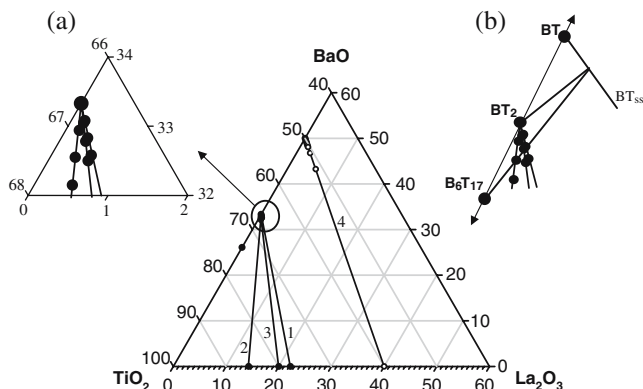
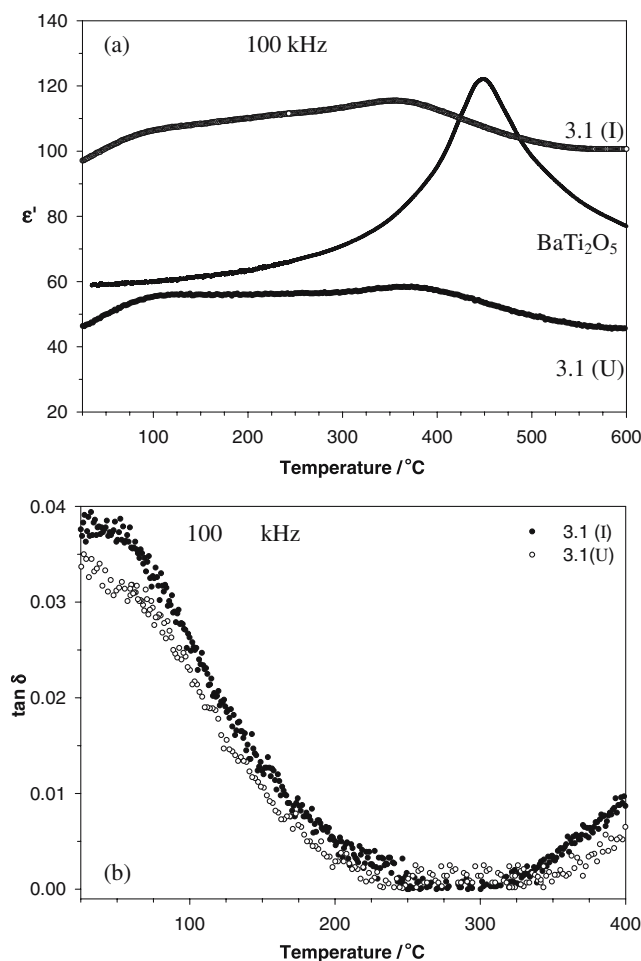


Fig. 6 (a) Composition triangle  $\text{BaO}-\text{TiO}_2-\text{La}_2\text{O}_3$  showing the compositions studied on joins 1 to 3 and the La-doped  $\text{BaTiO}_3$  solid solutions, join 4. (b) Crystallization products of La-doped  $\text{BaTiO}_3$  compositions. Since the  $\text{BT}_{ss}$  has variable La content, the results cannot be represented by a single compatibility triangle

BT<sub>2</sub> is sufficient to cause a reduction of  $T_c$  to 380–400 °C but is, nevertheless, <1%. From the decrease in  $T_c$  of BT with increasing  $x$ , it appears that a La-doped BT solid solution also forms. In samples 1.1, 2.1 and 3.1, the permittivity data indicate a  $T_c$  maximum of ~100 °C and therefore, an  $x$  value in the formula Ba<sub>1-x</sub>La<sub>x</sub>Ti<sub>1-x/4</sub>O<sub>3</sub> of approximately  $x=0.018$ . In sample 1.2, the  $T_c$  value is ~56 °C and  $x\approx 0.03$ . In all other compositions, however, the permittivity maximum for the BT phase is below room temperature and therefore,  $x>0.025$ . We have no information as to whether La is also able to enter the B<sub>6</sub>T<sub>17</sub> crystal lattice.

These results, in which the La contents ( $x$  values) in the BT solid solution, BTss, are higher than the overall  $x$  values of series 1, 2 and 3, are further evidence that the La is primarily located in the BT phase with little or none in B<sub>6</sub>T<sub>17</sub> but some in BT<sub>2</sub>, as evidenced by the reduction in  $T_c$  of BT<sub>2</sub>. The effect of addition of La to BT<sub>2</sub> is, therefore, to destabilise the BT<sub>2</sub> structure, leading to mixtures of B<sub>6</sub>T<sub>17</sub> and BTss. Although it is unlikely that the samples had reached thermodynamic equilibrium, the existence of three-phase assemblages: BTss, BT<sub>2</sub> and B<sub>6</sub>T<sub>17</sub> can be understood in terms of the compatibility triangle shown schematically in Fig. 6(b). On addition of La to BT<sub>2</sub>, on any of the joins 1, 2 and 3, the samples enter a 3-phase triangle BT<sub>2</sub>ss+B<sub>6</sub>T<sub>17</sub>+BTss; however the composition of the BTss varies inside this 3-phase triangle since the permittivity data show a variation in  $T_c$  and therefore in La content of BTss; consequently, the data are not consistent with a single triangle, which would be required under equilibrium conditions. With increasing La content, as well a change in BTss composition, the amount of BT<sub>2</sub> decreases leading, in compositions 1.3, 2.3 and 3.3, to 2-phase mixtures of B<sub>6</sub>T<sub>17</sub>+BTss.

Permittivity data are compared in Fig. 7 for a sample of undoped BT<sub>2</sub> [5] and a composition which has been chosen to have relatively temperature-independent permittivity over a wide range of temperatures. The latter sample is a composite containing grains of BT<sub>2</sub> interspersed with nano-sized grains of BT and is, therefore, a nanocomposite containing two ferroelectric phases with different compositions; it is well-established that on reducing the grain size in BT ceramics, the  $\epsilon'$  vs  $T$  plot becomes increasingly broadened; we observe a similar effect, which is why the term nanocomposite is used. A widely-used strategy to achieve temperature independent permittivity in electroceramic materials is to achieve a spread in  $T_c$  values, usually by means of achieving a spread in solid solution compositions. The results presented here provide a novel method to achieve such an effect by fabricating a sample containing a mixture of two different ferroelectric phases, one of which has nano-scale sized particles and the other which has an intrinsically broad permittivity versus temperature profile in polycrystalline samples. In addition, possibilities exist for the



**Fig. 7** (a) Permittivity data and (b)  $\tan \delta$  as a function of temperature at 100 kHz for undoped BT<sub>2</sub> [5] and sample 3.1 prepared by uniaxial (U) and isostatic (I) pressing

development of materials that meet X8R criteria for high temperature capacitor applications.

The results in Fig. 7 show that the permittivity maximum at ~430 °C in pure BT<sub>2</sub> is almost absent from the composite sample leading to temperature-independent permittivity over a wide temperature range. Further attention to ceramic processing conditions is required in order to maximise the permittivity; data are shown for a nanocomposite ceramic prepared by cold isostatic pressing, CIP, prior to sintering; the permittivity values are significantly higher than those for a similar sample prepared by uniaxial pressing prior to sintering.

#### 4 Conclusion

Nanocomposite ceramics containing a mixture of two ferroelectric phases, La-doped BaTi<sub>2</sub>O<sub>5</sub> and BaTiO<sub>3</sub>, with carefully-controlled phase amounts and ceramic microstruc-

ture have been prepared using a sol–gel process. The samples have temperature-independent permittivity and low dielectric loss over very wide temperature ranges:  $\epsilon' = 95 \pm 10$  from 25 to 600 °C;  $\tan \delta = 0.02(2)$  from 25 to 400 °C, measured at 100 kHz. The results presented here provide a novel method to achieve temperature independent permittivity in electroceramic materials.

**Acknowledgements** We thank the “Conselleria de Empresa, Universidad y Ciencia”—Project No. GV06/245, “Ministerio de Ciencia y Tecnología”—MAT 2002-02099 (HB, NM and EC), and the EPSRC (ARW) for financial support.

## References

1. T. Akashi, H. Iwata, T. Goto, *Mater. Trans.* **44**, 802 (2003)
2. T. Akashi, H. Iwata, T. Goto, *Mater. Trans.* **44**, 1644 (2003)
3. T. Kimura, T. Goto, H. Yamane, H. Iwata, T. Kajiwara, T. Akashi, *Acta Cryst.* **C59**, 1128 (2003)
4. Y. Akishige, K. Fukano, H. Shigematsu, *Jpn. J. Appl. Phys. (Part 2)* **42**, L946 (2003)
5. H. Beltrán, B. Gómez, N. Masó, E. Cordoncillo, P. Escribano, A. R. West, *J. Appl. Phys.* **97**, 084104-1 (2005)
6. K.W. Kirby, B.A. Wechsler, *J. Am. Ceram. Soc.* **74**, 1841 (1991)
7. D.E. Rase, R. Roy, *J. Am. Ceram. Soc.* **38**, 102 (1955)
8. W.O. Statton, *J. Chem. Phys.* **19**, 33 (1951)
9. E. Tillmanns, *Acta Cryst.* **B30**, 2894 (1974)
10. J.J. Ritter, R.S. Roth, J.E. Blendell, *J. Am. Ceram. Soc.* **69**, 155 (1986)
11. Y. Xu, G. Huang, H. Long, *Mater. Lett.* **57**, 3570 (2003)
12. S. Tangjuank, T. Tunkasiri, *Appl. Phys. A* **81**, 1105 (2005)
13. Y. Akishige, *Jpn. J. Appl. Phys.* **44**, 7144 (2005)
14. Y. Akishige, K. Fukano, H. Shigematsu, *J. Electroceramics* **13**, 561 (2004)
15. Y. Akishige, H. Shigematsu, A. Kitahara, I. Takahashi, *J. Korean Phys. Soc.* **46**, 24 (2005)
16. H. Beltrán, E. Cordoncillo, P. Escribano, D.C. Sinclair, A.R. West, *J. Appl. Phys.* **98**, 094102-1 (2005)
17. H. Beltrán, E. Cordoncillo, P. Escribano, D.C. Sinclair, A.R. West, *J. Am. Ceram. Soc.* **87**, 2132 (2004)
18. F.D. Morrison, D.C. Sinclair, A.R. West, *J. Appl. Phys.* **86**, 6355 (1999)